analytical chemistry

pubs.acs.org/ac Article

Novel Enhanced Lanthanide Electrochemiluminescence Luminophores: Ce^{3+}-Doped $TbPO_4$ Facile Synthesis and Detection for Mucin1

Cun Wang, Qian Han, Pingkun Liu, Gui Zhang, Li Song, Xiaochuan Zou, and Yingzi Fu*

Cite This: https://doi.org/10.1021/acs.analchem.1c01916 Read Online

ACCESS | Metrics & More | Article Recommendations | Supporting Information

ABSTRACT: Despite the upsurging interest in electrochemiluminescence (ECL) of lanthanides, the research in this field is still in its infancy due to the low intensity. In this work, a series of Ce^{3+}-doped terbium orthophosphates ($TbPO_4$:Ce) in different proportions have been synthesized through the co-precipitation method at room temperature. Meanwhile, through the investigation of morphologies and ECL properties of these $TbPO_4$:Ce, it is concluded that the ECL intensity reaches the maximum when the molar ratio of Tb/Ce is 9:1 and the material is nanorod-shaped. The ECL intensity of $TbPO_4$:Ce is significantly improved by doping with Ce^{3+} due to the dual sensitization strategy of the antenna effect from PO_4^{3-} to Tb^{3+} and the energy transfer from Ce^{3+} to Tb^{3+}. Interestingly, doping with Ce^{3+} can not only adjust morphology of $TbPO_4$:Ce but also improve the ECL intensity. In addition, to verify the application of $TbPO_4$:Ce, two single mucin1 (MUC1) aptamers are linked together to form a dual MUC1 aptamer chain. Then, a simple and sensitive ECL biosensor is constructed for the detection of MUC1, which can recognize the double amount of MUC1 and quench the ECL signal. As expected, the proposed biosensor shows good stability and acceptable selectivity and achieves sensitive detection of MUC1 with a dynamic range from 1 fg·mL^{-1} to 10 ng·mL^{-1} and a limit of detection of 0.5 fg·mL^{-1}. This work may pave a new avenue for the study of direct ECL emission of lanthanides and prove to be ideal for the research of new ECL luminophores in electrochemical analysis.

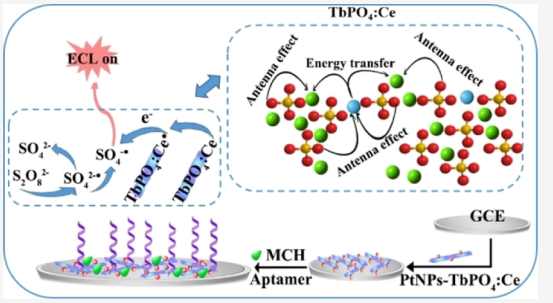

Electrochemiluminescence (ECL), a vital analytical technique combining electrochemistry and chemiluminescence, is endowed with high sensitivity, good selectivity, and simplicity.[1] A luminescent substance (luminophore) plays an irreplaceable role in the construction of ECL sensors.[2] The classical inorganic, organic, and nanomaterial luminophores have been comprehensively reported. However, the ECL intensity and efficiency of these luminophores still require further breakthrough. Therefore, it is urgent for the development of a new generation of luminescent materials. Lanthanide [Ln(III)] brings new opportunities in the synthesis of new generation luminescent materials ascribed to its intriguing optical properties and characteristics, such as long luminescence lifetime even a few microseconds, narrow emission bands, and large stokes shift.[3,4] Nevertheless, the application of Ln(III) in ECL sensors is still in its infancy. The direct ECL emission of Ln(III) is still difficult due to the intraconfigurational forbidden f → f transitions and low absorption coefficients.[5] To resolve these problems and improve the ECL intensity of Ln(III), various ligands possessing the "antenna effect", such as phenanthridine, 5-boronoisophthalic acid, and porphyrin, were introduced to absorb energy and transfer the energy to Ln(III).[6−8] The antenna effect of ligands can sensitize the ECL emission of the Ln(III) because the ligands reach the singlet state under the excitation of photons and then form a triplet state through the intersystem crossing process. At last, the energy transfers from the triplet state to Ln(III), resulting in the strong emission of Ln(III).[9,10] Meanwhile, various Ln(III) coordination polymers including lanthanide metal organic gels,[11,12] $EuPO_4$ nanowire,[13] and lanthanide terbium complex $Tb_2(C_6NO_2H_4)_6(H_2O)_4$[14] have been innovatively synthesized and applied to the construction of ECL sensors. As far as we know, although the ECL intensity of Ln(III) has been enhanced by the ligand antenna effect, it still needs to be further improved in ECL sensors for direct application. Recently, Ce^{3+} has been used as a sensitizer for Tb^{3+} due to the energy transfer between them (Ce^{3+} → Tb^{3+}).[4,15] Hence, the novel lanthanide luminophore of Ce^{3+}-doped $TbPO_4$ ($TbPO_4$:Ce) has been synthesized with different proportions through co-precipitation method at room temperature in this work. Meanwhile, the ligand antenna effect from PO_4^{3-} to Tb^{3+} and energy transfer (Ce^{3+} → Tb^{3+}) give rise to a dual sensitization effect, which is expected to further enhance

Received: May 6, 2021
Accepted: August 19, 2021

Scheme 1. Synthesis Process and ECL Mechanism of $TbPO_4$:Ce

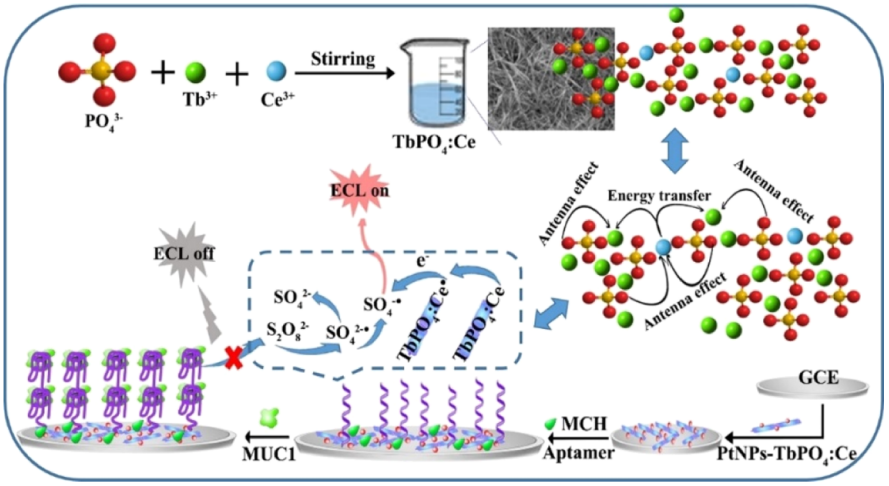

the ECL emission of $TbPO_4$:Ce and promote the application of Ln(III) (Tb^{3+}) in ECL sensors.

Mucin 1 (MUC1) is a type I transmembrane glycoprotein with a molecular weight of >200 kD.[16] Because MUC1 is closely related to the occurrence and development of tumors, it is considered to be a crucial potential biomarker for the diagnosis of early cancers such as prostate, ovarian, breast, pancreatic, and colorectal cancers.[17,18] At present, several ECL biosensors based on the 2D Zr12-adb nanoplate,[19] 3D DNA nanomachine,[20] and silver nanoparticles[21] have been reported for ultrasensitive detection of MUC1. Although, the development of the MUC1 ECL sensor has been promoted, the exploitation of more stable and sensitive ECL sensors is still of surging significance.

Herein, a novel, robust, and sensitive ECL biosensor has been fabricated for the detection of MUC1 by using $TbPO_4$:Ce (9:1) as the luminophore, potassium persulfate ($K_2S_2O_8$) as an efficient coreactant, and MUC1 as the quenching target analyte. Interestingly, the dual sensitization strategy consisting of the ligand antenna effect (from PO_4^{3-} to Tb^{3+}) and the energy transfer (from Ce^{3+} to Tb^{3+}) significantly increases the ECL intensity of $TbPO_4$:Ce, allowing Ln(III) (Tb^{3+}) to be directly applied to ECL sensors. Besides, two single MUC1 aptamers are innovatively linked together to form a dual aptamer chain, which can recognize double amount of MUC1 and quench the ECL signal. The results show that the proposed ECL biosensor has high sensitivity and successfully achieves rapid and efficient detection of MUC1, indicating the potential application of the proposed ECL biosensor in the detection of cancer-related biomarkers.

EXPERIMENTAL SECTION

Reagents and Apparatus. Terbium(III) nitrate hexahydrate [$Tb(NO_3)_3{\cdot}6H_2O$, 99.99%], cerium nitrate hexahydrate [$Ce(NO_3)_3{\cdot}6H_2O$, 99.9%], phosphine hydrochloride (TCEP, ≥98%), chloroauric acid ($H_2PtCl_6{\cdot}6H_2O$, ≥37.50% Pt basis), sodium dihydrogen phosphate ($NaH_2PO_4{\cdot}2H_2O$, ≥99%), 6-mercapto-1-hexanol (MCH), sodium borohydride ($NaBH_4$, 99%), and chitosan (25 g, average M.W. 100000−300000) were obtained from J&k Chemical Co. (Beijing, China). The DNA hybridization and stock solution was 20 mmol·L^{-1} Tris−HCl buffer (pH 7.4), containing 140 mmol·L^{-1} NaCl, 5 mmol·L^{-1} KCl, and 1 mmol·L^{-1} $MgCl_2$. The phosphate buffer saline (PBS, 0.1 mol·L^{-1} and pH 7.4) was prepared by mixing Na_2HPO_4 and KH_2PO_4 in different proportions with 0.1 mol·L^{-1} KCl as supporting electrolyte. The oligonucleotide sequences 5′−SH−$(CH_2)_6$ GCAGCAGTTGATCCTTTGGATACCCTGGTGTTTTTTGCAGCAGTTGATCCTTTGGATACCCTGGTG−$(CH_2)_6$−5′ were synthesized by Sangon Biotech. Co., Ltd. (Shanghai, China). Healthy human serum samples were supplied by the Ninth People's Hospital of Chongqing, China. All other chemicals were of analytical grade. Double distilled water was used in all experiments.

Electrochemical and ECL measurements were carried out on a CHI 604D electrochemical workstation (Shanghai Chenhua Instruments Co., China) and a model MPI-E electrochemiluminescence analyzer (Xi′an Remex Analysis Instruments Co. Ltd., Xi′An, China), respectively. During the ECL test, the potential sweep ranged from 0 to −2.0 V and the photomultiplier tube (PMT) was set at 650 V. A three-electrode system was used in all measurements, which was composed of a bare or modified glassy carbon electrode (GCE, Φ = 4.0 mm) as the working electrode, a platinum wire as the counter electrode, and an Ag/AgCl electrode (saturated KCl) as the reference electrode. The ECL measurements were performed in 3 mL of 0.1 mol·L^{-1} potassium persulfate ($K_2S_2O_8$, 0.1 mol·L^{-1} PBS and pH 7.4), unless otherwise specified. Scanning electron microscopy (SEM) images were acquired on a field emission Scanning electron microscope (ZEISS, Germany). The photoluminescence property study was carried out on a F7000 fluorescence spectrophotometer (Hitachi High-TechScience Co., Tokyo, Japan). X-ray photoelectron spectroscopy (XPS) was carried out using a thermos escalab 250Xi spectrometer (0−5000 eV, Thermo Electron Corporation, America). X-ray diffraction (XRD) was performed with an X-ray powder diffractometer (Brucker D8 ADVANCE, Germany). The ECL emission spectrum was recorded on a Newton electron-multiplying charge-coupled device (EMCCD) spectroscopy detector (Andor Co., England) combined with an electrochemical workstation based on a conventional three-electrode system.

Synthesis of $TbPO_4$:Ce with Different Proportions. As depicted in Scheme 1, Ce^{3+}-doped $TbPO_4$ ($TbPO_4$:Ce) was synthesized through co-precipitation method at room temperature. $TbPO_4$:Ce with different proportions (the molar ratio of Tb/Ce was 9:1, 9:3, 9:5, and 9:7) was synthesized as follows.[22] A mixture of $Tb(NO_3)_3{\cdot}6H_2O$ (0.09 mmol) and $Ce(NO_3)_3{\cdot}$

https://doi.org/10.1021/acs.analchem.1c01916
Anal. Chem. XXXX, XXX, XXX−XXX

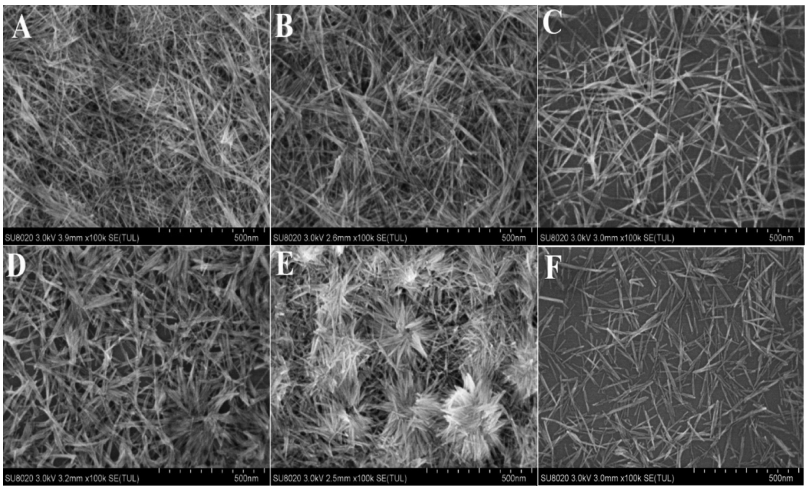

Figure 1. SEM images of (A) $TbPO_4$, (B) $TbPO_4$:Ce (9:1), (C) $TbPO_4$:Ce (9:3), (D) $TbPO_4$:Ce (9:5), (E) $TbPO_4$:Ce (9:7), and (F) $CePO_4$ (The content in brackets is the molar ratio of Tb/Ce).

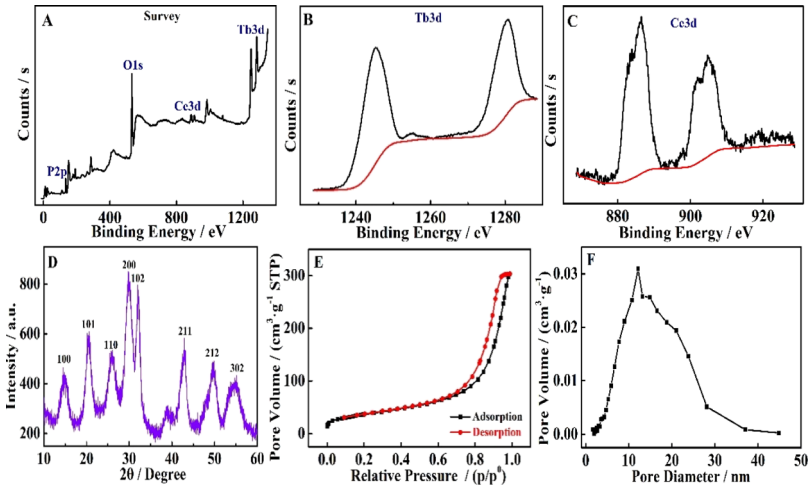

Figure 2. (A–C) XPS, (D) XRD, (E) N_2 adsorption and desorption isotherms (77 K), and (F) pore size distribution analysis of $TbPO_4$:Ce.

$6H_2O$ (0.01, 0.03, 0.05, and 0.07 mmol) was added in a beaker (100 mL) containing 20 mL of H_2O. Then, the mixture was stirred for 10 min to obtain a clear solution at room temperature. Subsequently, $NaH_2PO_4{\cdot}2H_2O$ (0.2 mmol) was added to the above solution and stirred for 3 h. The clear solution turned turbid, and a white precipitate was obtained immediately. Finally, the precipitate was centrifuged at 5000 rpm for 1 min, washed successively with water, and dried in air for further use. $TbPO_4$ and $CePO_4$ were prepared without adding $Ce(NO_3)_3{\cdot}6H_2O$ and $Tb(NO_3)_3{\cdot}6H_2O$.

Synthesis of Platinum nanoparticles. Platinum nanoparticles (PtNPs) were prepared according to the literature.[23] Briefly, 1.0 mL of trisodium citrate (1%) was rapidly added to 100 mL of boiling chloroplatinic acid (H_2PtCl_6, 0.01%) solution under vigorous stirring. The color of the solution turned black immediately. After stirring for 10 min, the obtained PtNPs were collected by centrifugation at 12000 rpm for 5 min, washed with water, and stored at 4 °C for further use.

Preparation of the $TbPO_4$:Ce-Modified Electrodes. Before using, the bare glassy carbon electrode (GCE) was continuously polished with 0.3 and 0.05 μm of alumina slurry and then ultrasonically cleaned with ethanol and water. A luminescent nanocomposite was obtained by mixing $TbPO_4$:Ce (9:1 and 2.0 mg) and PtNPs (2.0 mg) in 1 mL of chitosan solution (CS, 0.5%, Figure S1, see the Supporting Information) and stirring at room temperature for 3 h. Then, 5 μL of the above luminescent nanocomposite (2.0 mg·mL^{-1}) was dropped on the polished GCE to get a $TbPO_4$:Ce-modified electrode (denoted as $TbPO_4$:Ce/GCE). Next, the double MUC1 aptamer was dropped on $TbPO_4$:Ce/GCE and incubated overnight at 4 °C (aptamer/$TbPO_4$:Ce/GCE). After the non-specific binding sites were blocked with 10 μL of MCH (2 μmol·L^{-1}), various concentrations of MUC1 were dropped on aptamer/$TbPO_4$:Ce/GCE and incubated at 37 °C for 1 h. As the concentration of MUC1 increases, the ECL signal decreases. Finally, $TbPO_4$/GCE, $TbPO_4$:Ce (9:3)/GCE, $TbPO_4$:Ce (9:5)/GCE, $TbPO_4$:Ce (9:7)/GCE, and $CePO_4$/GCE were obtained in the similar way as the control.

RESULTS AND DISCUSSION

Manufacturing Process of the ECL Biosensor. Prior to ECL biosensor manufacturing, the influence of doping with Ce^{3+} in $TbPO_4$ was explored. The ECL responses of $TbPO_4$/GCE, $TbPO_4$:Ce (9:1)/GCE, $TbPO_4$:Ce (9:3)/GCE, $TbPO_4$:Ce (9:5)/GCE, $TbPO_4$:Ce (9:7)/GCE, and $CePO_4$/GCE are recorded in Figure S2. Because the highest ECL

https://doi.org/10.1021/acs.analchem.1c01916
Anal. Chem. XXXX, XXX, XXX−XXX

intensity was obtained from the $TbPO_4$:Ce (9:1)/GCE, $TbPO_4$:Ce (9:1) was selected as the ECL luminophore for further experiments. Meanwhile, no ECL-enhancement effect of PtNPs was found (Figure S3).

We used $TbPO_4$:Ce (9:1) as a luminophore, $K_2S_2O_8$ as a coreactant, and MUC1 as the quenching target analyte to design an ECL system (Scheme 1). This system owns the following merits: First, the dual sensitization strategy consisting of ligand antenna effect from PO_4^{3-} to Tb^{3+} and the energy transfer from Ce^{3+} to Tb^{3+} could significantly improve the ECL intensity of $TbPO_4$:Ce. Second, a dual MUC1 aptamer chain was designed to fix on the surface of the electrode, which could capture more MUC1 by forming a MUC1-aptamer complex and quench the ECL signal. Therefore, a highly sensitive ECL biosensor is expected to be achieved for the detection of MUC1. This is because of the steric hindrance effect of protein, which hinder the effective contact between coreactant and the luminophore, resulting in a low ECL signal.

Characterization of $TbPO_4$:Ce. SEM was applied to characterize the morphologies of $TbPO_4$:Ce in different molar ratios. Pure $TbPO_4$ (Figure 1A) and $CePO_4$ (Figure 1F) exhibit the morphologies of nanofibers and nanorods, respectively, with a diameter of about 800 and 200 nm. The morphologies of $TbPO_4$:Ce (9:1), $TbPO_4$:Ce (9:3), $TbPO_4$:Ce (9:5), and $TbPO_4$:Ce (9:7) gradually changed from nanorods to nanoflowers. The diameter was about 600, 400, 300, and 300 nm, respectively (Figure 1B–E).

As shown in Figure 2A–C, the XPS peaks at 133.2 and 531.1 eV belong to P 2p and O 1s, respectively. Besides, the double peaks at 1245.3 and 1280.7 eV are derived from Tb 3d. The peaks of Ce 3d are 886.5 and 906.2 eV, respectively, indicating that Ce^{3+} was successfully doped in $TbPO_4$. The crystal structure of $TbPO_4$:Ce was detected by XRD. All diffraction peaks in XRD can be perfectly assigned to the hexagonal cell of $TbPO_4$ or $CePO_4$ (Figure 2D). Compared with pure $CePO_4$ [Joint Committee on Powder Diffraction Standards (JCPDS) card no. 34-1380] and $TbPO_4$ (JCPDS card no. 20-1244), the peak positions of $TbPO_4$:Ce shift slightly for a slight difference in the radius of Ce^{3+} and Tb^{3+} [r(Tb) < r(Ce)]. These results are consistent with the literature.[24,25] Figure 2E illustrates the N_2 adsorption and desorption isotherms of $TbPO_4$:Ce. The specific surface area of $TbPO_4$:Ce was calculated as 130.63 $m^2 \cdot g^{-1}$ and total pore volume was 0.4690 $cm^3 \cdot g^{-1}$ from Brunauer–Emmett–Teller (BET) method. These results reveal that $TbPO_4$:Ce owns the characteristic of a type-IV isotherm. In Figure 2F, $TbPO_4$:Ce exhibits a nanopore structure, and the pore size was calculated as 12.1 nm by the Barrett–Joyner–Halenda (BJH) method.- The $TbPO_4$:Ce was also investigated by energy dispersive X-ray (EDX) spectroscopy and the result is shown in Figure S4. All above characterizations indicate that the preparation of $TbPO_4$:Ce is successful.

The fluorescence properties of $TbPO_4$:Ce and $TbPO_4$ were tested upon excitation at 256 nm. As shown in Figure 3A, compared with pure $TbPO_4$, four strong emission peaks are observed at different wavelengths, which correspond to $^5D_4 \rightarrow {}^7F_J$ (J/6, 5, 4, and 3) transitions of Tb^{3+} ($^5D_4 \rightarrow {}^7F_6$ at 491.6 nm, $^5D_4 \rightarrow {}^7F_5$ at 550 nm, $^5D_4 \rightarrow {}^7F_4$ at 586.2 nm, and $^5D_4 \rightarrow {}^7F_3$ at 622.4 nm). The weak and broad band emission (d–f radiative transition) between 300 and 400 nm corresponds to Ce^{3+} in the $TbPO_4$:Ce.[26,27] Energy can be effectively transferred from the wide band emitter to the narrow line

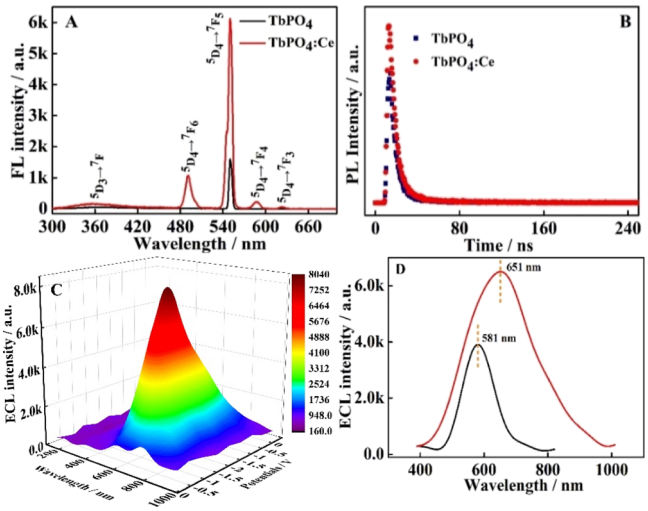

Figure 3. (A) FL emission spectra and (B) time-resolved PL decay curve of $TbPO_4$ and $TbPO_4$:Ce, (C) 3D ECL spectrum of the $TbPO_4$:Ce/GCE, and (D) 2D ECL spectra of the bare GCE and $TbPO_4$:Ce/GCE in 0.1 mol·L^{-1} $S_2O_8^{2-}$ (pH 7.4).

emitter when spectral overlap between the neighboring ions in the material exists.[28] In the case of Ce^{3+}-doped $TbPO_4$, the energy of the Ce^{3+} excited state can be transferred to the energy level of Tb^{3+} ($4f^n$), resulting in an f–d transition.[29] This is to say that energy can be transferred from Ce^{3+} to Tb^{3+}; thus the fluorescence intensity of $TbPO_4$:Ce is enhanced. Figure 3B displays that the PL lifetime (τ_{ave}) of $TbPO_4$:Ce (23.63 ns) is about 2.56 ns longer than that of pure $TbPO_4$ (21.04 ns), indicating that the PL emission characteristic of $TbPO_4$:Ce is improved after doping with Ce^{3+}. Meanwhile, the 3D and the 2D ECL spectra of the $TbPO_4$:Ce/$S_2O_8^{2-}$ system were also analyzed, which provide a new perspective for studying the ECL characteristics of $TbPO_4$:Ce. As shown in Figure 3C,D, the maximum ECL emission wavelength of the $TbPO_4$:Ce/$S_2O_8^{2-}$ system ($S_2O_8^{2-}$ as a coreactant) is 651 nm, which is about 70 nm red-shifted compared with the ECL emission of the $O_2/S_2O_8^{2-}$system.

Possible ECL Mechanism of $TbPO_4$:Ce. The performances of ECL and cyclic voltammetry (CV) of the bare GCE and $TbPO_4$:Ce/GCE were investigated. On the bare GCE, no apparent ECL signals (Figure 4A a) and redox peaks (Figure 4Aa′) are observed in 0.1 mol·L^{-1} PBS (pH 7.4), while a weak ECL signal (Figure 4Ab) and a cathode current peak (Figure 4Ab′) at −1.23 V are observed in 0.1 mol·L^{-1} $S_2O_8^{2-}$ (pH 7.4). For $TbPO_4$:Ce/GCE, a small ECL signal (Figure 4Ba) and no redox peaks (Figure 4Ba′) are obtained in 0.1 mol·L^{-1} PBS (pH 7.4); however, a strong ECL signal (Figure 4Bb) and an obvious cathode current peak (Figure 4Bb′) at −1.30 V are acquired in 0.1 mol·L^{-1} $S_2O_8^{2-}$ (pH 7.4). A cathode current peak is obtained on the bare GCE in $S_2O_8^{2-}$ solution, suggesting that $S_2O_8^{2-}$ can be reduced to $SO_4^{\bullet-}$ (radical ion) at cathodic potential (eqs 2 and 3). On the $TbPO_4$:Ce/GCE, the phenomena of a weak ECL signal emerged in PBS and a strong ECL signal observed in $S_2O_8^{2-}$ (Figure 4Ab,Bb), indicating that $TbPO_4$:Ce can gain electrons and generate the radical ion $(TbPO_4:Ce)^{\bullet-}$ (eq 1). Then, $(TbPO_4:Ce)^{\bullet-}$ reacts with $SO_4^{\bullet-}$ to form the excited state $(TbPO_4:Ce)^*$ (eq 4). The ECL emission occurs when $(TbPO_4:Ce)^*$ decays from the excited state back to the ground state $TbPO_4$:Ce (eq 5). After removing the dissolve oxygen (O_2) from the test solution, the

https://doi.org/10.1021/acs.analchem.1c01916
Anal. Chem. XXXX, XXX, XXX–XXX

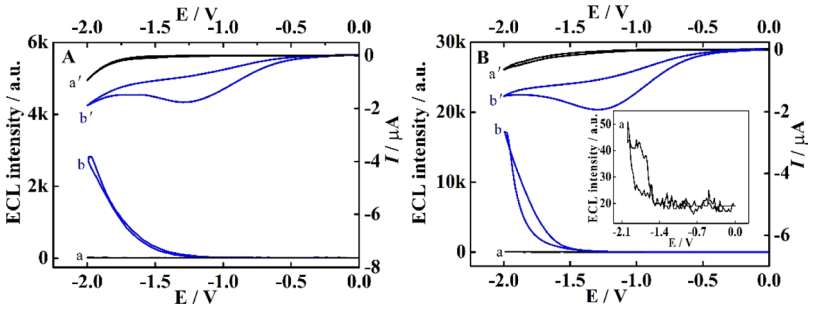

Figure 4. ECL (a,b) and CV (a′,b′) performances of the (A) bare GCE and (B) $TbPO_4$:Ce/GCE in (a,a′) 0.1 mol·L^{-1} PBS (pH 7.4) and (b,b′) 0.1 mol·L^{-1} $S_2O_8^{2-}$ (pH 7.4).

ECL intensity dropped by about 1069 a.u. (Figure S5). So, O_2 can slightly enhance the ECL intensity of the $TbPO_4$:Ce/$S_2O_8^{2-}$ system in this work.[9,30−32]

The ECL mechanism of the $TbPO_4$:Ce/$S_2O_8^{2-}$ system is detailed as follows[9]

$$TbPO_4\text{: Ce} + \vec{e}(TbPO_4\text{: Ce})^{\bullet -} \quad (1)$$

$$SO_8^{2-} + \vec{e}SO_4^{2\bullet -} \quad (2)$$

$$SO_4^{2\bullet -} + \vec{e}SO_4^{\bullet -} + SO_4^{2-} \quad (3)$$

$$(TbPO_4\text{: Ce})^{\bullet -} + SO_4^{\bullet -}(TbPO_4\text{: Ce})^{*} + SO_4^{2-} \quad (4)$$

$$(TbPO_4\text{: Ce})^{*} \rightarrow TbPO_4\text{: Ce} + h\nu \quad (5)$$

Analytical Performance of the ECL Sensor. Electrochemical impedance spectroscopy (EIS) and CV were applied to investigate the preparation process of the modified electrodes (Figure S6). Under the optimal experimental conditions (Figure S7), the ECL signals were recorded by incubating MUC1 at different concentrations to assess the applicability of the obtained ECL biosensors. As shown in Figure 5, the ECL intensity decreased with the gradually

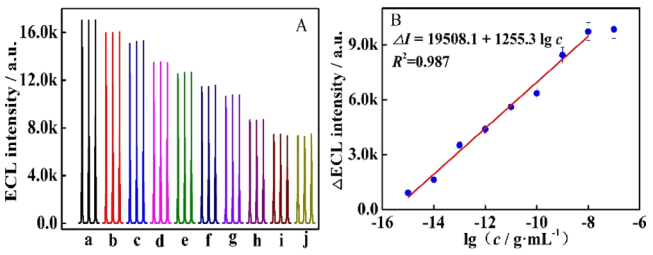

Figure 5. (A) ECL intensity and (B) calibration plot of the biosensor for different concentrations of MUC1: (a) 0, (b) 1 fg·mL^{-1} (c) 10 fg·mL^{-1}, (d) 100 fg·mL^{-1}, (e) 1 pg·mL^{-1}, (f) 10 pg·mL^{-1}, (g) 100 pg·mL^{-1}, (h) 1 ng·mL^{-1}, (i) 10 ng·mL^{-1}, and (j) 100 ng·mL^{-1}.

increasing concentration of MUC1 from 1 fg·mL^{-1} to 10 ng·mL^{-1}. The change in ECL intensity ($\Delta I = I_{blank} - I$, where I_{blank} and I represent the ECL intensities of $TbPO_4$:Ce/GCE incubation with blank and various MUC1 concentrations, respectively) is linearly related to the logarithmic concentration of MUC1, and the regression equation is ΔI = 19508.1 + 1255.3 lg c (R^2 = 0.987). The detection limit of MUC1 is 0.5 fg·mL^{-1} (S/N = 3), which is better than that of other reported methods (Table S1).

Selectivity, Stability, and Reproducibility of the ECL Biosensor. To investigate the performance of the designed biosensor comprehensively, the selectivity, stability, and reproducibility of the biosensor were evaluated in detail. First, several interfering substances, such as alpha fetoprotein (AFP), prostate specific antigen (PSA), carcinoembryonic antigen (CEA), human albumin (HSA), bovine serum albumin (BSA), and hemoglobin (Hb) were selected to assess the selectivity of the proposed biosensor. As shown in Figure 6A, the ECL response of the interfering substances (1 μg·mL^{-1}) are similar to that of the blank. Oppositely, a remarkably decreased ECL signal is obtained for the proposed biosensor incubated with the target MUC1 (10 ng·mL^{-1}) or the mixture (1 μg·mL^{-1} interfering substances mixed with 10 ng·mL^{-1} MUC1). The obtained results prove the high selectivity of the elaborated biosensor. Next, as seen in Figure 6B, there is no significant difference in ECL signals after consecutive scanning for 1000 s and the relative standard deviation (RSD) is 0.48%, indicating the satisfactory stability of the ECL biosensor. Meanwhile, the RSD of intra-assay and inter-assay of $TbPO_4$:Ce/GCE was calculated to be 0.83 and 1.1%, respectively (Figure 6C), demonstrating the acceptable reproducibility of the biosensor. In addition, the ECL intensity of the modified biosensor decreased by only 0.1% after 1 month of storage at room temperature. Besides, the biostability of the biosensor was evaluated by detecting 1 and 100 fg·mL^{-1} MUC1 in 0.1 mol·L^{-1} $S_2O_8^{2-}$ (0.1 mol·L^{-1} PBS and pH 7.4) and 100 pg·mL^{-1} and 100 fg·mL^{-1} MUC1 in healthy human serum samples (0.1 mol·L^{-1} PBS and pH 7.4 containing 0.1 mol·L^{-1} $S_2O_8^{2-}$) under a continuous scan for 11 cycles. As depicted in Figure S8, the ECL biosensor signal did not change significantly and the RSD were 0.81, 0.72, 1.1, 1.2%, indicating the good biostability of the proposed biosensor. All the above results show that our proposed biosensor owns good and acceptable selectivity, stability, and reproducibility.

Application of the Biosensor. The applicability of the designed biosensors had been assessed for real samples. Before testing, the healthy human serum samples were centrifuged and then the supernatant was diluted 50 times with 0.1 mol·L^{-1} PBS (pH 7.4). Subsequently, different concentrations of MUC1 were added in the real samples and measured using the standard addition method using the modified biosensor. The recovery varied from 90.0−107.0% (RSD ≤ 1.4%), which is acceptable (Table S2, Supporting Information).

CONCLUSIONS

In summary, a series of Ce^{3+}-doped $TbPO_4$ ($TbPO_4$:Ce) in different proportions have been synthesized through co-precipitation method at room temperature. Impressively, the dual sensitization strategy composed of the ligand antenna effect and the energy transfer increases the ECL intensity of

https://doi.org/10.1021/acs.analchem.1c01916
Anal. Chem. XXXX, XXX, XXX−XXX

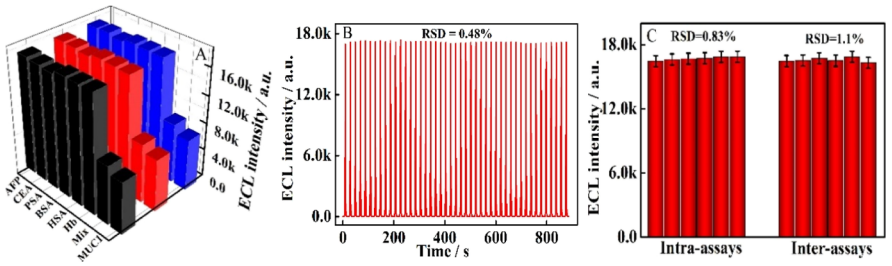

Figure 6. (A) Selectivity evaluation of the $TbPO_4$:Ce/GCE for 10 ng·mL^{-1} MUC1 and 1 μg·mL^{-1} interfering ions (AFP, CEA, PSA, BSA, HSA, or Hb). (B) ECL stability of the $TbPO_4$:Ce/GCE under consecutive cyclic potential scans for 1000 s in 0.1 mol·L^{-1} $S_2O_8^{2-}$ (pH 7.4). (C) Reproducibility (intra-assays and inter-assays, n = 6) of the $TbPO_4$:Ce/GCE for 1 fg·mL^{-1} MUC1.

$TbPO_4$:Ce, which enables the lanthanides to be directly applied in ECL sensors. In terms of application, a simple and sensitive ECL sensing platform for MUC1 detection is also constructed based on $TbPO_4$:Ce as a luminophore and MUC1 as a high-efficiency quenching target analyte. This work may present a grand avenue to achieve a strong ECL signal from lanthanides, which gives a fresh impetus to the construction of new generation of ECL luminophores with potential applications in the biological analysis.

■ ASSOCIATED CONTENT

Supporting Information

The Supporting Information is available free of charge at https://pubs.acs.org/doi/10.1021/acs.analchem.1c01916.

Effect of the concentrations of chitosan on the performance of modified electrodes, ECL intensity of different $TbPO_4$:Ce compositions, effect of PtNPs for the ECL intensity, EDX of $TbPO_4$:Ce, influence of dissolved oxygen (O_2) on the ECL performance, electrochemical performance of the stepwise modified electrodes, optimization of $TbPO_4$:Ce/GCE with different pH values, ECL biostability of the proposed biosensor, and different methods for the detection of MUC1 and application of the proposed biosensor (PDF)

■ AUTHOR INFORMATION

Corresponding Author

Yingzi Fu − *Key Laboratory of Luminescence Analysis and Molecular Sensing (Southwest University), Ministry of Education, School of Chemistry and Chemical Engineering, Southwest University, Chongqing 400715, China;* orcid.org/0000-0003-4894-8549; Phone: +86-023-68252277; Email: fyzc@swu.edu.cn

Authors

Cun Wang − *Key Laboratory of Luminescence Analysis and Molecular Sensing (Southwest University), Ministry of Education, School of Chemistry and Chemical Engineering, Southwest University, Chongqing 400715, China; School of Biological and Chemical Engineering, Chongqing University of Education, Chongqing 400067, PR China*

Qian Han − *Key Laboratory of Luminescence Analysis and Molecular Sensing (Southwest University), Ministry of Education, School of Chemistry and Chemical Engineering, Southwest University, Chongqing 400715, China; College of Resources and Environment Science, Hebei Normal University, Shijiazhuang 050024 Hebei, China*

Pingkun Liu − *Key Laboratory of Luminescence Analysis and Molecular Sensing (Southwest University), Ministry of Education, School of Chemistry and Chemical Engineering, Southwest University, Chongqing 400715, China*

Gui Zhang − *Key Laboratory of Luminescence Analysis and Molecular Sensing (Southwest University), Ministry of Education, School of Chemistry and Chemical Engineering, Southwest University, Chongqing 400715, China*

Li Song − *Key Laboratory of Luminescence Analysis and Molecular Sensing (Southwest University), Ministry of Education, School of Chemistry and Chemical Engineering, Southwest University, Chongqing 400715, China*

Xiaochuan Zou − *Key Laboratory of Luminescence Analysis and Molecular Sensing (Southwest University), Ministry of Education, School of Chemistry and Chemical Engineering, Southwest University, Chongqing 400715, China*

Complete contact information is available at: https://pubs.acs.org/10.1021/acs.analchem.1c01916

Notes

The authors declare no competing financial interest.

■ ACKNOWLEDGMENTS

The authors gratefully acknowledge the financial support from the National Natural Science Foundation of China (22077105), the Natural Science Foundation Project of CQ CSTC (cstc2020jcyj-msxmX0854), the Children's Research Institute of National Center for Schooling Development Programme and Chongqing University of Education (CRIKT202021), and the Key Laboratory for Green Chemical Technology of Chongqing University of Education, China (2016xjpt08).

■ REFERENCES

(1) Du, Y.; Xue, J.; Sun, X.; Wu, D.; Liu, X.; Ju, H.; Yang, L.; Wei, Q. *Anal. Chem.* **2020**, *92*, 8472−8479.
(2) Li, L.; Chen, Y.; Zhu, J.-J. *Anal. Chem.* **2017**, *89*, 358−371.
(3) Wang, H.-S.; Bao, W.-J.; Ren, S.-B.; Chen, M.; Wang, K.; Xia, X.-H. *Anal. Chem.* **2015**, *87*, 6828−6833.
(4) Zeng, H.-H.; Zhang, L.; Rong, L.-Q.; Liang, R.-P.; Qiu, J.-D. *Biosens. Bioelectron.* **2017**, *89*, 721−727.
(5) da Silva, C. M.; Ellena, J.; Frem, R. C. G. *New J. Chem.* **2020**, *44*, 10146−10152.
(6) Heffern, M. C.; Matosziuk, L. M.; Meade, T. J. *Chem. Rev.* **2014**, *114*, 4496−4539.
(7) Chen, F.; Wang, Y.-M.; Guo, W.; Yin, X.-B. *Chem. Sci.* **2019**, *10*, 1644−1650.
(8) Jiang, Z. W.; Zou, Y. C.; Zhao, T. T.; Zhen, S. J.; Li, Y. F.; Huang, C. Z. *Angew. Chem., Int. Ed.* **2020**, *59*, 3300−3306.
(9) Werts, M. H. V. *Sci. Prog.* **2005**, *88*, 101−131.

(10) Cui, Y.; Yue, Y.; Qian, G.; Chen, B. *Chem. Rev.* **2012**, *112*, l126−1162.
(11) Li, Y.; Jiang, Z. W.; Xiao, S. Y.; Huang, C. Z.; Li, Y. F. *Anal. Chem.* **2018**, *90*, 12191−12197.
(12) Wang, C.; Han, Q.; Liu, P.; Zhang, G.; Song, L.; Zou, X.; Fu, Y. *ACS Sens.* **2021**, *6*, 252−258.
(13) Ma, H.; Zhou, J.; Li, Y.; Han, T.; Zhang, Y.; Hu, L.; Du, B.; Wei, Q. *Biosens. Bioelectron.* **2016**, *80*, 352−358.
(14) Yang, Y.; Zhang, Y.; Shu, G.; Dong, Q.; Zou, L.; Zhu, Y. *J. Lumin.* **2015**, *159*, 73−78.
(15) Kuang, X.-y.; Liu, H.; Hu, W.-y.; Shao, Y.-z. *Dalton Trans.* **2014**, *43*, 12321−12328.
(16) Jiang, X.; Wang, H.; Wang, H.; Yuan, R.; Chai, Y. *Anal. Chem.* **2016**, *88*, 9243−9250.
(17) Li, J.; Liu, J.; Bi, Y.; Sun, M.; Bai, J.; Zhou, M. *Anal. Chim. Acta* **2020**, *1105*, 87−94.
(18) Yuan, J. -L.; lv, Z.; Liu, Z.-G.; Hu, Z. *J. Mol. Sci.* **2007**, *191*, 104−113.
(19) Yao, L.-Y.; Yang, F.; Hu, G.-B.; Yang, Y.; Huang, W.; Liang, W.-B.; Yuan, R.; Xiao, D.-R. *Biosens. Bioelectron.* **2020**, *155*, 112099.
(20) Jiang, X.; Wang, H.; Wang, H.; Zhuo, Y.; Yuan, R.; Chai, Y. *Anal. Chem.* **2017**, *89*, 4280−4286.
(21) Wei, Y.-P.; Zhang, Y.-W.; Mao, C.-J. *J. Mater. Chem. B* **2020**, *8*, 2471−2475.
(22) Carrasco, I.; Piccinelli, F.; Romet, I.; Nagirnyi, V.; Bettinelli, M. *J. Phys. Chem. C* **2018**, *122*, 6858−6864.
(23) Goenka, S.; Toussaint, J. *Cosmetics* **2020**, *7*, 88−102.
(24) Di, W.; Willinger, M.-G.; Ferreira, R. A. S.; Ren, X.; Lu, S.; Pinna, N. *J. Phys. Chem. C* **2008**, *112*, 18815−18820.
(25) Bu, W.-B.; Hua, Z.-L.; Zhang, L.-X.; Chen, H.-R.; Huang, W.-M.; Shi, J.-L. *J. Mater. Res.* **2004**, *19*, 2807−2811.
(26) Guo, H. *Appl. Phys.* **2006**, *84*, 365−369.
(27) Lai, H.; Bao, A.; Yang, Y.; Tao, Y.; Yang, H.; Zhang, Y.; Han, L. *J. Phys. Chem. C* **2008**, *112*, 282−286.
(28) Li, Q.; Yam, V. W.-W. *Angew. Chem., Int. Ed.* **2007**, *46*, 3486−3489.
(29) Erdei, S.; Ainger, F. W.; Ravichandran, D.; White, W. B.; Cross, L. E. *Mater. Lett.* **1997**, *30*, 389−393.
(30) Xu, Z.-H.; Wang, H.; Wang, J.; Zhao, W.; Xu, J.-J.; Chen, H.-Y. *Anal. Chem.* **2019**, *91*, 12000−12005.
(31) Reshetnyak, O. V.; Koval'chuk, E. P.; Skurski, P.; Rak, J.; Błażejowski, J. *J. Lumin.* **2003**, *105*, 27−34.
(32) Yao, W.; Wang, L.; Wang, H.; Zhang, X. *Electrochim. Acta* **2008**, *54*, 733−737.

https://doi.org/10.1021/acs.analchem.1c01916
Anal. Chem. XXXX, XXX, XXX−XXX